AD-A144 889 SHIPBOARD MEASUREMENT OF CLOUD BASES AND AVERAGE SURFACE VISIBILITY WITH AN EYE-SAFE LIDAR(U) NAVAL RESEARCH LAB WASHINGTON DC W P HOOPER 09 AUG 84 1/1

UNCLASSIFIED NRL-8819 SBI-AD-E000 589 F/G 20/5 NL

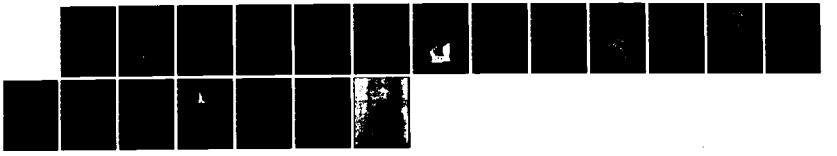

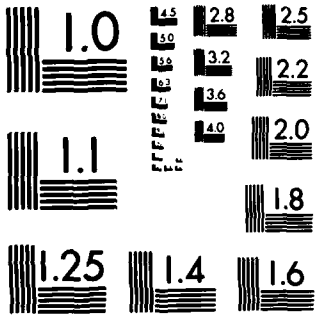

NRL Report 8819

Shipboard Measurement of Cloud Bases and Average Surface Visibility with an Eye-Safe Lidar

WILLIAM P. HOOPER

Atmospheric Physics Branch
Space Science Division

August 9, 1984

NAVAL RESEARCH LABORATORY
Washington, D.C.

AD-A145 [illegible]

SECURITY CLASSIFICATION OF THIS PAGE

REPORT DOCUMENTATION PAGE

1a REPORT SECURITY CLASSIFICATION UNCLASSIFIED	1b RESTRICTIVE MARKINGS
2a SECURITY CLASSIFICATION AUTHORITY	3 DISTRIBUTION/AVAILABILITY OF REPORT Approved for public release; distribution unlimited.
2b DECLASSIFICATION/DOWNGRADING SCHEDULE	
4 PERFORMING ORGANIZATION REPORT NUMBER(S) NRL Report 8819	5 MONITORING ORGANIZATION REPORT NUMBER(S)
6a NAME OF PERFORMING ORGANIZATION Naval Research Laboratory 6b OFFICE SYMBOL (If applicable)	7a NAME OF MONITORING ORGANIZATION
6c ADDRESS (City, State and ZIP Code) Washington, DC 20375	7b ADDRESS (City, State and ZIP Code)
8a NAME OF FUNDING/SPONSORING ORGANIZATION Naval Ocean Systems Center 8b OFFICE SYMBOL (If applicable)	9 PROCUREMENT INSTRUMENT IDENTIFICATION NUMBER
8c ADDRESS (City, State and ZIP Code) San Diego, CA 92152	10 SOURCE OF FUNDING NOS PROGRAM ELEMENT NO: 62759N; PROJECT NO: WF59551B; TASK NO: ; WORK UNIT NO: DN639-124
11 TITLE (Include Security Classification) (see page ii)	
12 PERSONAL AUTHOR(S) Hooper, William P.	
13a TYPE OF REPORT Interim 13b TIME COVERED FROM TO	14 DATE OF REPORT (Yr, Mo, Day) 1984 August 9 15 PAGE COUNT 19
16 SUPPLEMENTARY NOTATION	
17 COSATI CODES FIELD / GROUP / SUB GR	18 SUBJECT TERMS (Continue on reverse if necessary and identify by block number) Eye-safe lidar; Surface visibility Cloud base height; Shipboard lidar

19 ABSTRACT (Continue on reverse if necessary and identify by block number)

An eye-safe lidar, originally built by a Navy contractor, has been modified by the Naval Research Laboratory and evaluated at sea. The instrument operated in the severest weather encountered, a moderate gale. Cloud bases below 2 km and visibilities less than 10 km were measured. Improvements are needed to reduce sky noise and increase receiver sensitivity, but the system is surprisingly resistant to ocean spray and shipboard vibration.

20 DISTRIBUTION AVAILABILITY OF ABSTRACT UNCLASSIFIED UNLIMITED ☒ SAME AS RPT ☐ OTIC USERS ☐	21 ABSTRACT SECURITY CLASSIFICATION UNCLASSIFIED
22a NAME OF RESPONSIBLE INDIVIDUAL William P. Hooper	22b TELEPHONE NUMBER (Include Area Code) 202-767-3317 22c OFFICE SYMBOL Code 4112

DD FORM 1473, 83 APR EDITION OF 1 JAN 73 IS OBSOLETE

SECURITY CLASSIFICATION OF THIS PAGE

11. Title (Include Security Classification)

Shipboard Measurement of Cloud Bases and Average Surface Visibility with an Eye-Safe Lidar

CONTENTS

SHIPBOARD MEASUREMENT OF CLOUD BASES AND AVERAGE SURFACE VISIBILITY WITH AN EYE-SAFE LIDAR

INTRODUCTION

An eye-safe lidar operated by Warner [1] is measuring cloud-base height and estimating visibility along airplane glide paths at the Munich-Riem airport. Similar shipboard measurements would be useful for the Navy, but questions about lidar capabilities must be answered. Can a lidar routinely make measurements from a ship? An ocean-going ship exposes deck equipment to a harsh environment of salt spray and vibration. Can a lidar operate at sea for an extended period without intensive maintenance? At NRL we conducted 4 weeks of shipboard tests with a lidar similar to Warner's and provided some answers to these questions.

The NRL lidar uses a laser diode and a silicon avalanche photodiode for light emission and detection. They are extremely reliable, have minimum power requirements, and can be easily interfaced with electronics. Unfortunately, the spectral width of the laser diode is considerably wider than the width of most lasers that are used by lidars. Only a small contrast exists between the background sunlight and light from the laser diode; therefore, the resulting signal to sky noise ratio is small. During data acquisition, the NRL lidar averages the lidar returns to increase this ratio; nevertheless, this ratio is too small to allow Klett's [2] analytical method to be used. Instead, approximate methods are necessary to analyze lidar returns. In this report, a simple model estimates the average visibility in the surface layer.

Lidars that are not eye safe require extensive safeguards. These safeguards restrict hazardous lidars to controlled areas where air traffic is limited. The maximum permissible light intensity in an eye-safe laser beam increases dramatically as the wavelength changes from the visible ($\lambda < 0.7\ \mu$m) to the far infrared ($\lambda > 1.4\ \mu$m). Eye-safe lidars operating in the far infrared achieve the highest possible signal-to-noise ratio. Unfortunately, most lasers presently used operate in the visible and near infrared. Expanding the beams from these lasers reduces the light intensity to eye-safe levels. While a large expansion is difficult for narrow-beam lasers, it is easier for laser diodes which have a large beam divergence. To achieve eye safety, the laser beam for the NRL lidar has an initial diameter of 12 cm.

The characteristics of the NRL lidar contrast strongly with the lidar (visioceilometer) developed by Lentz [3] at the U.S. Army Atmospheric Sciences Laboratory. The NRL lidar occupies 1 m^3 and weights 100 kg; the visioceilometer is about 18 cm^3 and weights less than 4 kg. The visioceilometer analytically inverts the lidar return; the NRL lidar uses approximate techniques. The small optics of the visioceilometer (>2 cm) differ from the large optics of the NRL lidar and require careful alignment. The NRL lidar is not sealed like the visioceilometer and is repairable at sea. For shipboard applications, advantages and disadvantages of these instruments (or similar instruments) can best be discovered by oceanographic tests.

EQUIPMENT DESCRIPTION

The NRL lidar, originally built by Sperry Rand [4] to measure visibility and cloud-base heights, has been modified by personnel in the Atmospheric Physics Branch for use in field experiments. The lidar is coaxial, with the transmitter mounted in the center of the receiving optics, Figs. 1 and 2.

Manuscript approved February 6, 1984.

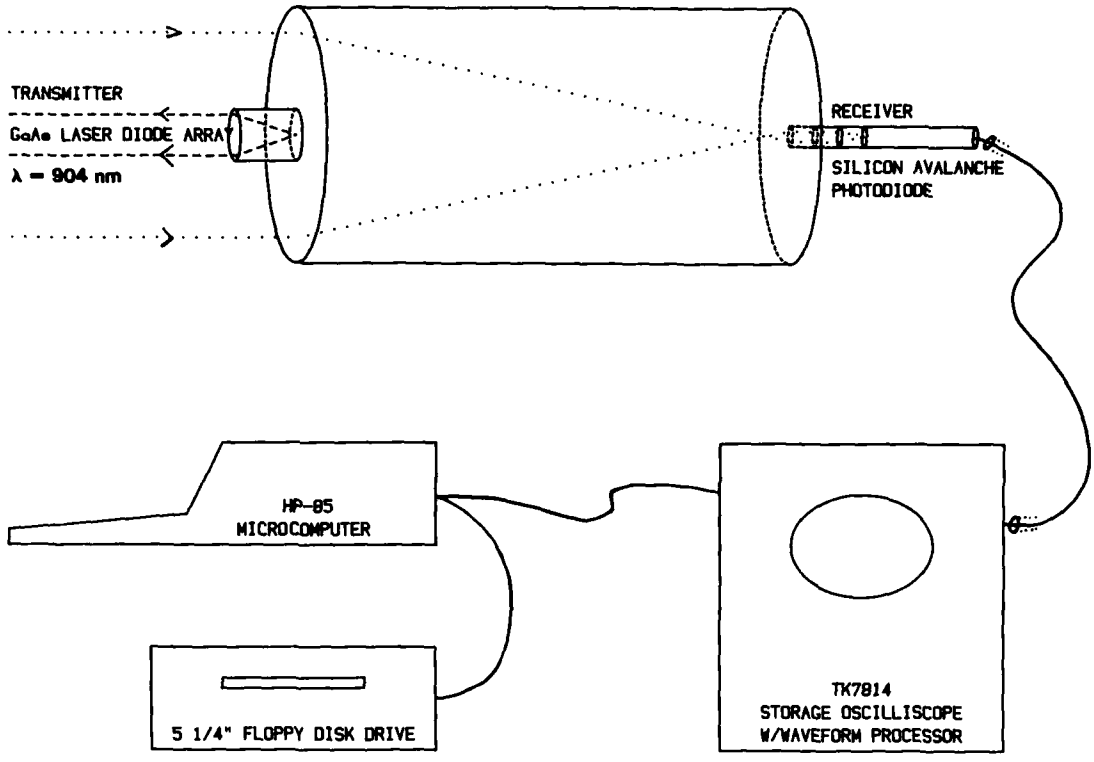

Fig. 1 — This schematic outlines the lidar system. At the top is the lidar. The bottom shows the oscilloscope, computer, and floppy disk drive used for data acquisition. The dashed line marks the path of the transmitted light; the dotted line illustrates the path of the light backscattered to the receiver. The line between the receiver and oscilloscope represents a coaxial line. An IEE-48 bus connects the oscilloscope, computer, and floppy disk drive.

R-1089

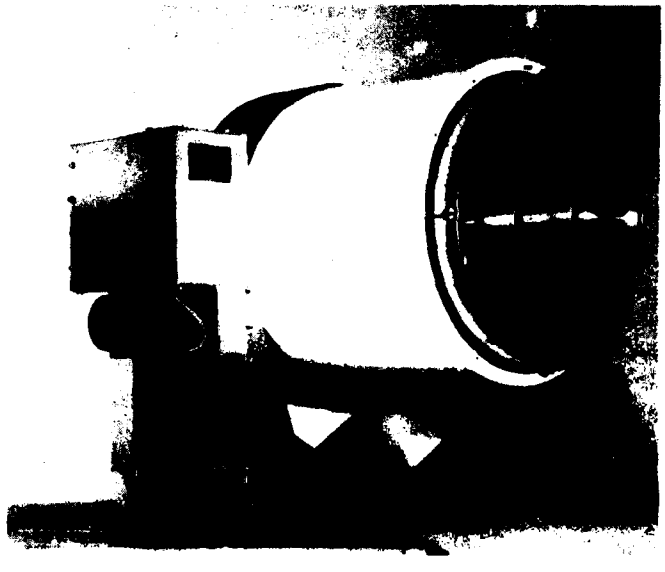

Fig. 2 — This photograph shows the NRL lidar. The transmitter is in the center. The collecting optics encircle the transmitter. The box on the left-hand side houses controls that allow the elevation angle of the lidar to be changed.

Simplicity and vibration resistance are provided by the solid-state transmitter and receiver sensors (Table 1). Fresnel optics used in the transmitter and receiver are inexpensive and lightweight but difficult to clean.

Table 1 – NRL lidar

Transmitter	
Laser	48 element GaAs diode array (Laser Diode Lab LD-235)
Wavelength	904 nm
Spectral Width	3.5 nm
Output Energy	400 W (2E-5 J/pulse)
Pulse Duration	50 ns
Pulse Repetition Rate	2 kHz
Lens Diameter	12.7 cm
Beam Divergence	20 mrad
Receiver	
Detector	Silicon avalanche photodiode (General Electric LE-103B)
Responsivity	3.3E+5 V/W
Spectral Bandwidth	10 nm
Lens Diameter	43.2 cm
Field of View	50 mrad
Data Acquisition	
Amplifier	Linear (50 dB)
Waveform Averager	Tektronix 7854
Processor	HP-85
Storage	5-1/2-in. (14-cm) floppy disk
Complete Unit	
Weight	113 kg (250 lb)
Size	91 cm – width 106 cm – length 66 cm – height

A few critical modifications were necessary to allow the instrument to measure visibility and cloud-base height. Optical fibers coupled the original lasers to the collimating lens. These lasers and fibers have been replaced by a small integrated GaAs array made by Laser Diode Laboratory. The receiver amplifier was replaced by high-speed operational amplifiers, improving the bandpass and dynamic range. The original water-damaged sky filter was also replaced.

The laser transmits 2000 light pulses a second at a wavelength of 904 nm. Each pulse is 50 ns in duration, with 400 W peak power. The transmitted light is collimated by a Fresnel objective lens 12.7 cm in diameter into a beam with a 20-mrad divergence. Since the spectral bandwidth of 3.5 nm is considerably broader than most typical narrow-bandwidth lasers, the lidar suffers from considerably more sky noise.

A Fresnel lens 40 cm in diameter collects the scattered light for the receiver. Two simple uncoated lenses collimate the light through a 10-nm-bandpass interference filter and focus the filtered light on a silicon avalanche diode. The diode, made by General Electric, is 3.2 mm in diameter, with a

sensitivity of 3.3×10^{-5} V/W. The electrical signal from the diode is amplified and passed through a coaxial cable to a waveform processor. This coaxial allows for easy coupling of the lidar aboard ship, and the signal processor can be located in a protected shipboard area away from the exposed deck-mounted lidar. The lidar signal is displayed, digitized, and averaged by a signal processor with a range resolution that can be varied from 1.5 to 15 m. This processor takes a few points from each lidar profile and gradually builds an average shape of the lidar return. The speed of this process depends on the range resolution used, but it typically requires a few minutes to average 1000 measurements at each range in a 512-point profile.

EYE SAFETY

The low-power laser and the broad transmitted laser beam of the NRL lidar provide eye safety. Maximum permissible exposure (MPE) for laser radiation is set by ANSI Z136.1 [5]. The individual pulse energy, not the average energy, determines the MPE for the NRL lidar. For a laser repetition rate of 1 kHz, with a wavelength of 904 nm, and a Gaussian laser pulse half width of 50 ns, the MPE is

$$H = 7.5 \times 10^{-8} \text{ J/cm}^2.$$

Assuming that the transmitted light uniformly fills the transmitter objective lens with a beam divergence of 20 mrad, the NRL lidar becomes eye safe at 3.8 m. When the lidar beam is viewed with 7×50 binoculars, this eye safe range increases to 48 m. Since the laser beam may not uniformly fill the transmitting lens, the eye-safe ranges are only approximate; nevertheless, the results indicate the eye safety potential for this instrument.

For remote lidar operation, the laser beam leaving the transmitting lens should be eye safe. Increasing the transmitting objective lens diameter and/or decreasing the laser power would make this beam safe. Interlocks would also be required to ensure that the laser did not operate with the transmitter case open.

RESULTS

From data from a 4-week cruise across the Atlantic (Fig. 3), measurements of cloud bases and visibility were made. Lidar data operate in two modes. First, profiles of lidar return are taken vertically with short time averages to measure the height of cloud bases. A range resolution of 15 m is used, yielding useful data to about 2 km. Second, the lidar is pointed horizontally (as horizontal as possible on a rolling ship) and lidar profiles are averaged for 5 min to estimate the visibility in the surface layer. Here the range resolution is 1.5 m and the maximum range is about 0.5 km.

Cloud-Base Measurements

Cloud-base heights were estimated from the height at which the power return was a local maximum. Four hundred of these measurements were made during the complete cruise. These heights were observed for the cloud bases of stratus, scud, and "fair weather" cumulus. The heights of stratus cloud bases at the beginning and the end of the cruise are discussed in this section to reveal the lidar capabilities under realistic shipboard conditions. Finally, the lidar observations are compared with radiosonde measurements.

As USNS *Lynch* left Charleston, S.C., a low formed off the coast of Cape Hatteras (see Fig. 4). Cold air streamed from the coast out over the ocean. The cloud bases shown in Fig. 5 start at about 600 m in Charleston and gradually increase to 1500 m as the cold air is warmed by the Gulf Stream. Then the bases' heights decrease with the approach of a rain storm. The total time scale is 36 h, and observations that appear to be simultaneous were separated by at least 10 min. The surface wind speeds were above 15 m/s during this period, and the cloud deck changed considerably in height for intervals as short as a few minutes. Although the variation in cloud height was not measured by other instruments, this variability appears to reflect the actual cloud height variation.

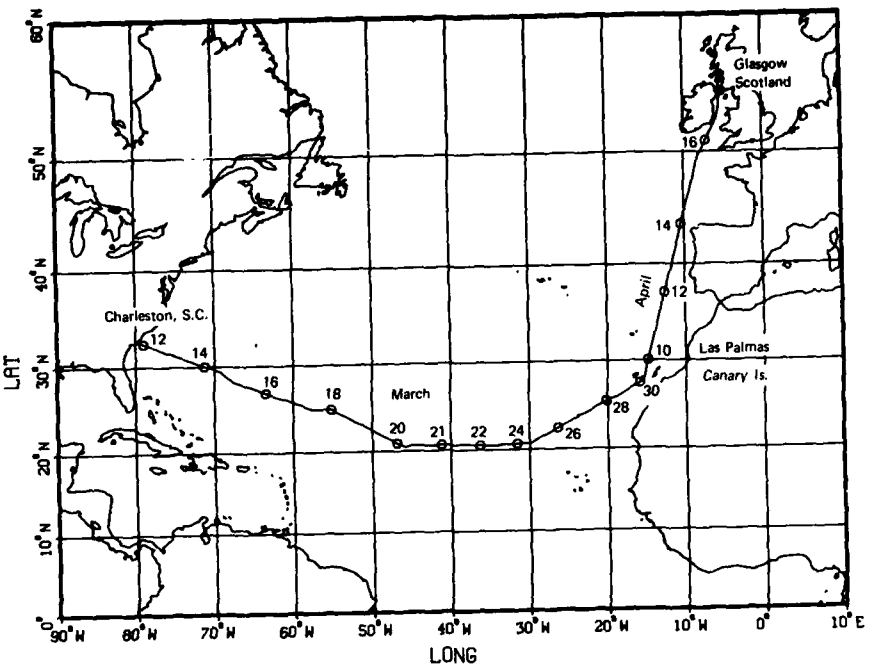

Fig. 3 — The 1983 cruise of the *Lynch* from Charleston, S.C. through Las Palmas, Canary Islands, to Glasgow, Scotland, is shown. The symbol (?) marks the beginning of every other day. We reached Las Palmas on March 31 and did not leave until April 9.

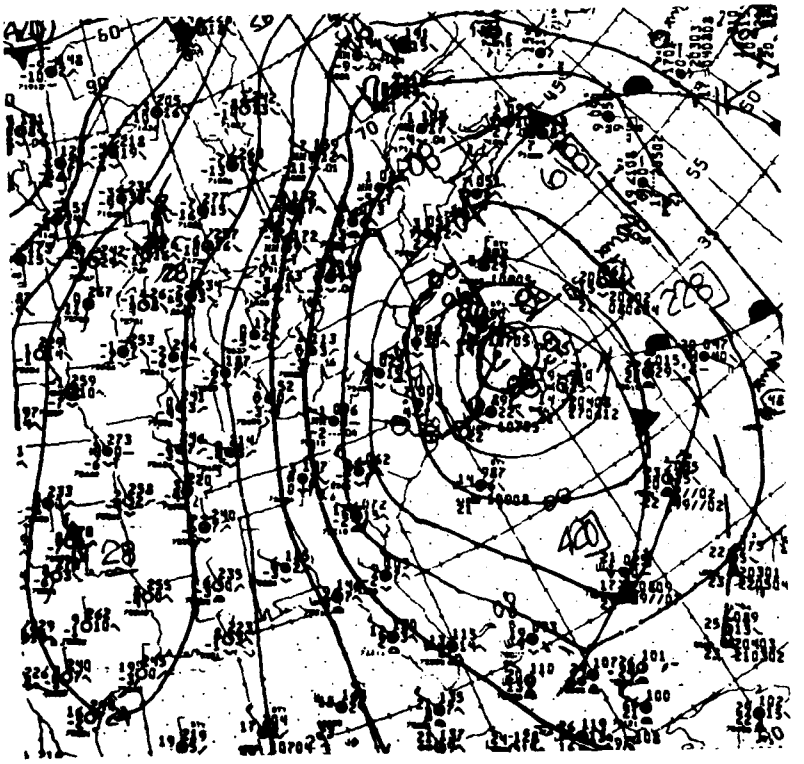

Fig. 4 — The weather map from 1800 GMT March 11 shows a low forming off the east coast of the United States

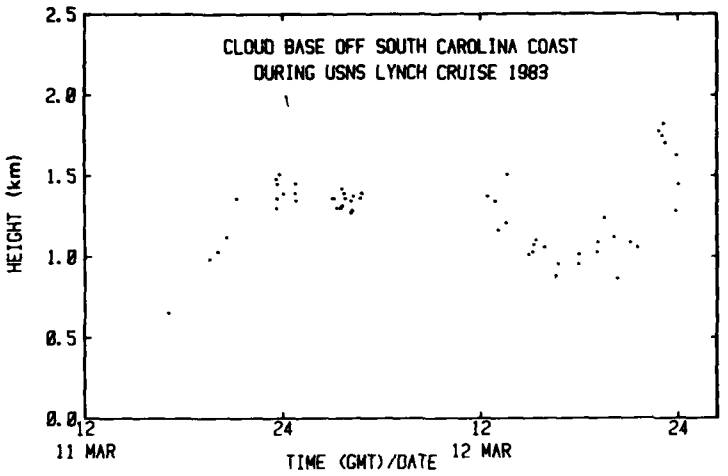

Fig. 5 — The cloud-base heights at the beginning of the cruise are plotted here. Each individual point represents an individual cloud-height measurement. A *low formed off Cape Hatteras* (Fig. 4). *The surface winds* were above 15 m/s during this period and were coming off the land over the sea. At first the cloud bases increase in height as the air is warmed by the Gulf Stream, then the cloud bases decrease with an approaching rain storm.

Figure 6 shows the cloud-base heights during a cold-frontal passage in the Irish Sea near the end of the cruise. These measurements were made two days after the ship encountered 12-ft (3.7-m) seas. The force of these waves as they broke over exposed decks caused extensive damage to experimental instruments. Except for the failure of the power cable, the lidar remained operational. The synoptic situation is shown in Fig. 7. The cloud-base heights begin at 300 m, gradually increase, and reach about 1000 m. The cloud base is periodically obscured by rain, allowing fewer observations after 1845 GMT.

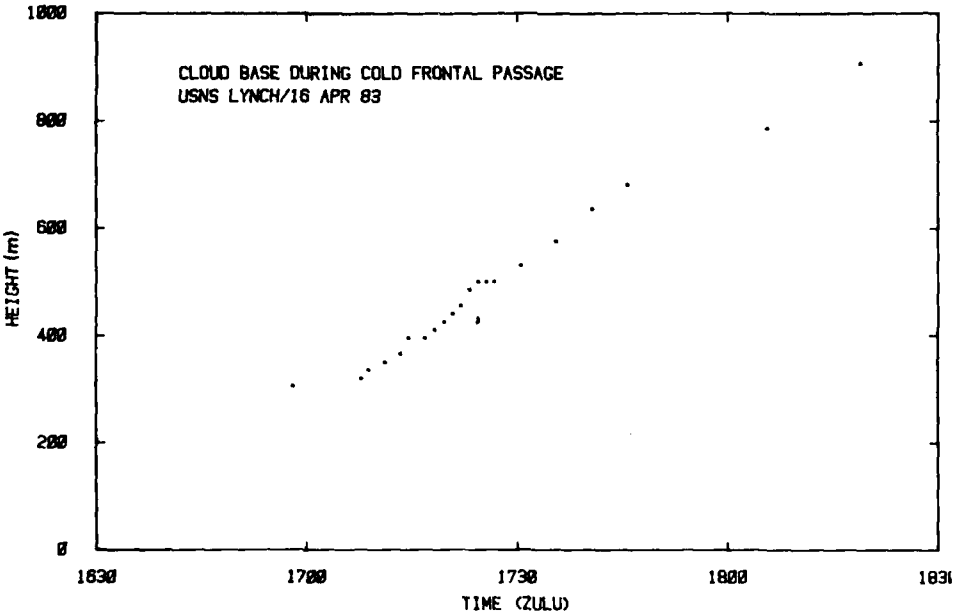

Fig. 6 — Near the end of the cruise a cold front passed over the USNS *Lynch* (Fig. 7). This figure shows the cloud-base heights during this passage. The winds were light at the beginning of the cold front passage but increased to 5 m/s by the end.

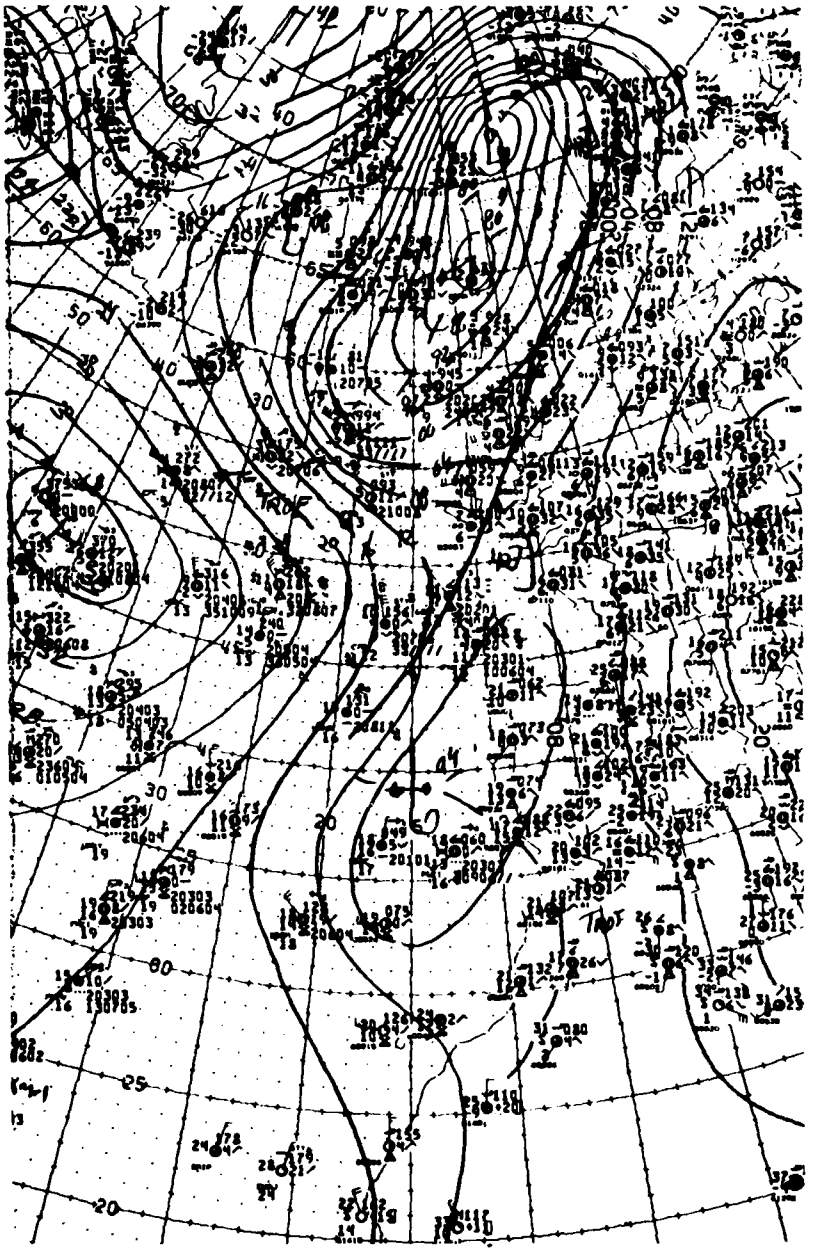

Fig. 7 — This weather map from April 16, 1983 at 1200 GMT shows a cold front passage over the Irish Sea

Dr. R. Helvey analyzed temperature and humidity soundings from the cruise [6]. I estimated the cloud base from these soundings to be the height of 97% relative humidity or the height of peak relative humidity (if less than 97%). The 97% correlation between lidar and radiosonde data is obvious in Fig. 8. The lidar heights are systematically higher than the radiosonde heights. The exact reason for this difference is not apparent, but possible errors include lidar range calibration and extended cloud penetration by the near-infrared radiation. This relatively small error can be removed by further radiosonde comparisons.

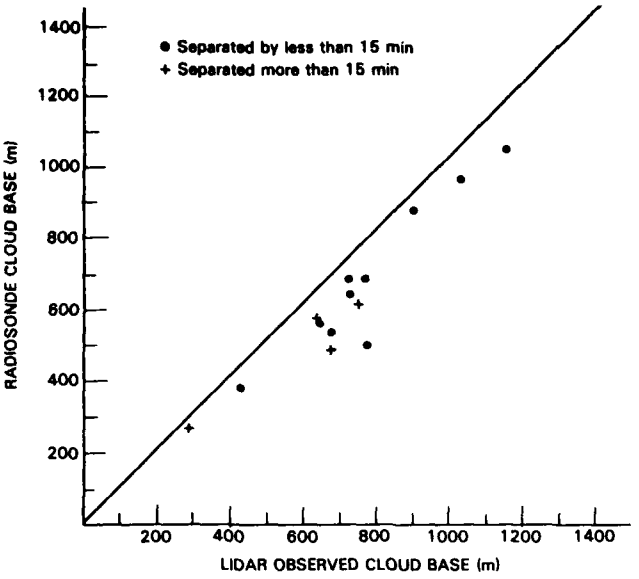

Fig. 8 — The lidar and radiosonde cloud base heights are compared. Dr R. Helvey provided the Temperature and relative humidity soundings from the cruise [6]. The radiosonde heights represent those at which the relative humidity reached 97% or was a maximum (if less than 97%).

Visibility Estimates

As range increases most lidars asymmetrically approach a relatively simple lidar equation given by Collis [7]. A modified form of this equation is

$$P(R) = \frac{E\, A_r c}{8\pi\, R^2}\, \beta_s(R)\, \mathbb{P}\,(180°,\, R)\, \exp\left[-2\int_0^R \beta_e\,(R')\,dR'\right], \tag{2}$$

where

R is the range,

$P(R)$ is the power return,

E is the energy per pulse,

A_R is the receiver area,

c is the speed of light,

$\beta_s(R)$ is the scattering cross section,

$\mathbb{P}(180°,\, R)$ is the backscatter phase function, and

$\beta_e(R)$ is the extinction cross section per unit volume.

At very close range, the lidar pulse shape and receiver function strongly effect the lidar return. A Gaussian laser pulse shape is assumed,

$$G(R) = \frac{1}{r\pi a_5} e^{-a_5 R^2}, \tag{3}$$

where a_5 is the half width of the Gaussian laser pulse.

For most lidars, including both Lentz's and Warner's, the laser transmitter and receiver are parallel but separated by a short distance; however, for the NRL lidar, the transmitter and receiver are coaxial. This unusual configuration coupled with the large beam divergence allows the transmitted lidar beam to enter the receiver field of view after traveling only a few meters. This distance is assumed to be small enough to allow the receiver junction to be approximated by the step function

$$H(R) = \begin{cases} 0, & R < a_6, \\ 1, & R > a_6, \end{cases} \tag{4}$$

where a_6 is the range at which the transmitted laser beam enters the receiver field of view.

Some of the data taken involved firing the lidar horizontally and averaging for several minutes. The atmosphere is assumed to be homogeneous:

$$P(R) = \frac{a_1 e^{-a_2 R}}{R_2}, \tag{5}$$

where a_1 is the amplitude of the return and a_2 is the average attenuation.

The power return of the NRL lidar represents a convolution of laser pulse shape [Eq. (3)] with the product of the homogeneous return [Eq. (5)] and receiver function [Eq. (4)]:

$$\tilde{P}(R - a_3) = \int_{-\infty}^{\infty} H(R) P(R) G(R - R') dR' + a_4, \tag{6}$$

where

$\tilde{P}$ is the model of the actual lidar return,

a_3 is the range offset between the data and model results, and

a_4 is the zero offset of the receiver amplifier.

The model is fitted to an averaged lidar return (see Fig. 9). The return pulse is flat when the oscilloscope is saturated. The length of the saturation region can be minimized; however, the accuracy of the digitation outside the saturation region decreases. The data taken in the saturation region are not used by the fitting procedure. The model incorporates six parameters (see Table 2). The half width of the laser pulse (a_5) and the closest range at which the laser pulse enters the receiver field of view (a_6) are estimated. The remaining parameters are determined by a nonlinear fitting subroutine from Bevington [8]. In Fig. 10 the current through the laser as a function of time is fitted by a Gaussian that provides an estimate of the laser pulse half width.

The closest range of received data is estimated both from laboratory and model experimentation. Lights are placed in both the receiver and the transmitter. At a range of 15 m from the lidar, both lights are seen; this range provides an experimental estimate of a_6.

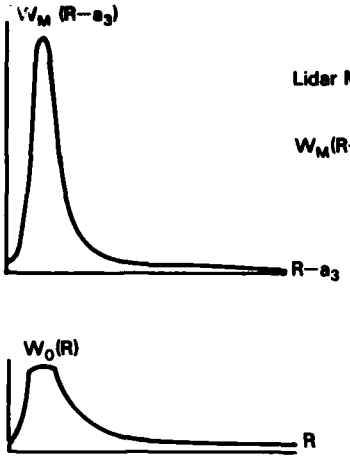

Lidar Model

$$W_M(R-a_3) = a_1 \int_{a_6}^{\infty} P(R')G(R'-R)dR + a_4$$

Fit Model to Observed Data by Minimizing:

$$E = \sum \left[W_0(R)-W_M(R-a_3)\right]^2$$

Fig. 9 — An actual and a model lidar return are shown. The lidar return from a homogeneous atmosphere is also shown. This return is convoluted with the laser pulse shape (see Fig. 10) to yield the model lidar return.

Table 2 — Model Parameters

Symbol	Parameter
a_1	Amplitude of lidar return
a_2	Attenuation of laser beam
a_3	Range offset between data and model
a_4	Zero offset of receiver amplifier
a_5	Half width of transmitted laser pulse
a_6	Range at which transmitted pulse enters receiver field of view

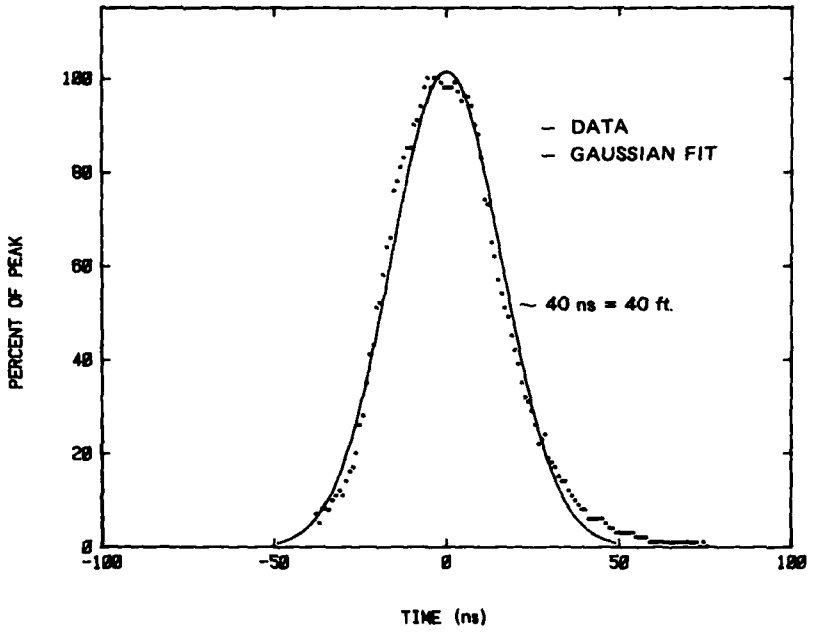

Fig. 10 — The laser pulse shape and a Gaussian fit to this shape are plotted. The vertical axis is proportional to the current through the laser. The Gaussian fit is used in the convolution model of the lidar return.

The nephelometer described in Ref. 9 measures the visibility at the spectral wavelength of the lidar. With this value used to fix the extinction in the model, a_6 could be estimated. This fitting was done for 40 lidar observations spread throughout the cruise period. For the first attempt, 25 m about the saturation region was omitted. Shown in Fig. 11 are the large width of the distribution and the disagreement of the average location with the experimental time with 50 m about the saturation region excluded. The results are also shown on Fig. 11 and agree with the experimental observations. The average of this distribution, 16.6 m, is used in the subsequent data analysis.

Visibility observations made by the lidar and by the nephelometer [9] are compared for data taken on the night of March 15/16. The period provides a test of lidar operation in the ocean environment. Visibility is restricted by intermittent light drizzle. The 8-ft (2.4-m) waves follow the vessel, and ocean spray occasionally covers the lidar. Scud clouds are observed by the lidar at about 450 m. Visibility is estimated from backscatter by the Koshmieder relationship,

$$V_r = \frac{3.92}{\beta} \tag{7}$$

where

V_r is the visibility and

β represents both the backscatter and the extinction coefficient.

The nephelometer and the lidar operate in the near infrared, and Eq. (7) estimates visibility only approximately; however, the visibility is calculated in the same way for both devices, and the results should be comparable.

Figure 12 shows the actual visibility comparisons. The visibility is high during this period except for two intervals with light drizzle, from 0100 to 0300 GMT and from 0700 to 1000 GMT. The

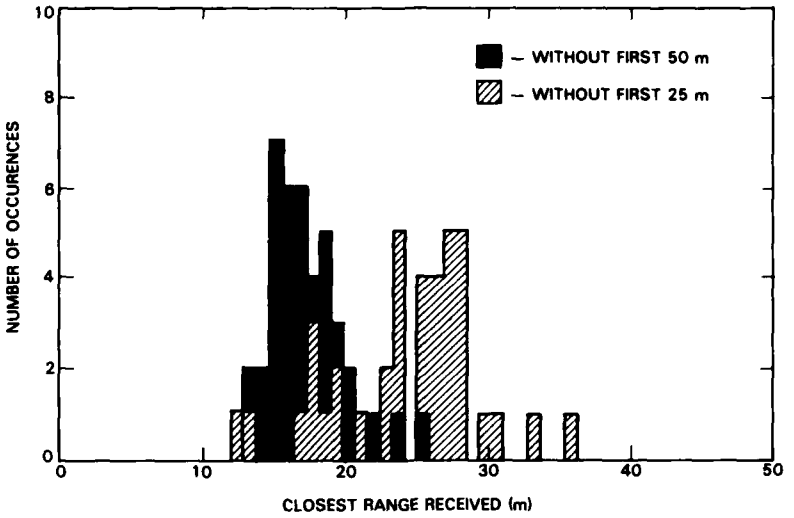

Fig. 11 — The convolution model of the lidar return has six parameters. One of these parameters represents the range at which the transmitted laser pulse is first observed by the receiver. This parameter, a_6, is determined by fitting the data for 40 independent data samples throughout the cruise. The horizontal axis shows the range increments. The vertical axis shows the number of times a range is observed in the 40 samples. The dashed histograms show the range distribution when 25 m about the saturation point of the oscilloscope is omitted. This distribution is broad, and the mean is considerable larger than the experimentally estimated value. A second histogram of fitted values is shown solid with 50 m about the saturation point removed. This distribution is narrower and has a mean of 16.6 m. The convolution model uses the second value, which is much closer to the expected value.

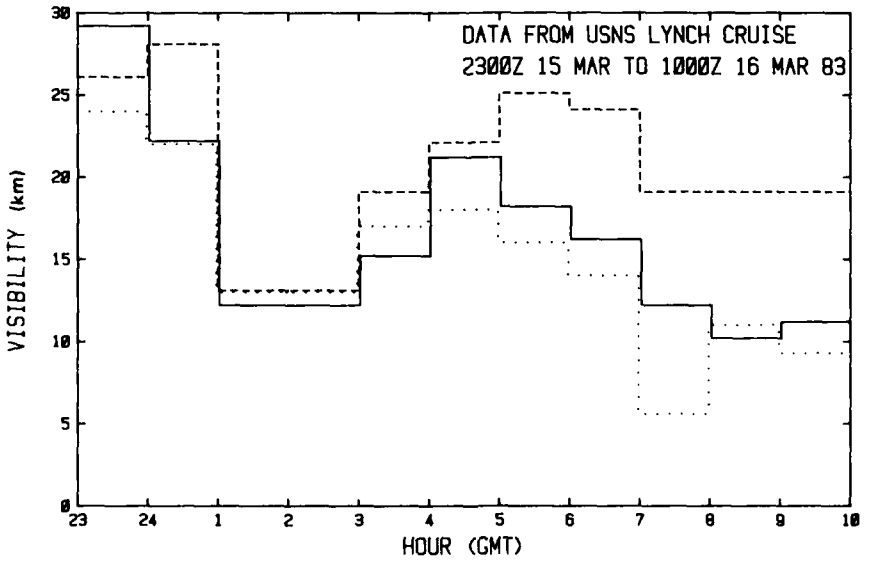

Fig. 12 — This figure compares the visibility measurements made by the HSS nephelometer [9] and the lidar. These measurements were made during a night when intermittent light drizzle fell. The solid line shows the measurements of the nephelometer. Lidar estimates from the amplitude a_1 are dashed, and lidar measurements from the attenuation a_2 are dotted. The lidar estimates are arbitrarily scaled to fall on top of the nephelometer observations. These estimates diverged from the other measurements as rain drops collected on the external lidar optics, changing the lidar constant.

nephelometer data, although continuous, have been averaged into hourly segments. The 5-min averages of lidar profiles were made every 15 min; hourly averages generally include four observations. The lidar visibility was estimated from the amplitude of the return (a_1). This parameter is proportional to backscatter and system constants. The observations were arbitrarily scaled to fall on top of the nephelometer measurements. This lidar visibility estimate did reasonably well until 0500 GMT, when rain drops collected on the lens surfaces, changing the system constants. An absolute measurement of the visibility was also estimated from the model-generated extinction coefficient. System constants do not directly affect this estimate, and the estimate does not need to be scaled. This measurement compares poorly during clear periods when the lidar signal is small; but it compares well during periods of restricted visibility when the backscatter is stronger. Between 0700 and 0800 GMT, one lidar observation occurred during heavier rain. When this observation is excluded, the lidar hourly average compares well with the nephelometer result. The good agreement between lidar extinction and nephelometer observations between 0700 and 1000 GMT is especially encouraging, since the rain drops were collecting on the external lidar optics.

CONCLUSIONS

The NRL lidar has been successfully used at sea. During the Atlantic cruise, measurements were made on 26 out of 28 possible days. The instrument is rugged, eye safe, and simple. During a moderate gale, the lidar operated until a board came loose on the deck and severed the power cable. Cloud heights can be measured within and at the top of the maritime boundary layer. The simple model explained in the Visibility Estimates section allows average visibilities in the surface layer to be estimated. The estimates are accurate during periods of restricted visibility below 10 km. This type of instrument can measure visibility and cloud base when these observations are most needed by the Navy.

Improvements should be made to increase the sensitivity and reduce the sky noise of this lidar, but the large optics are not strongly affected by ocean spray. Daily cleaning of the external optics surfaces was done during the cruise. The use of a windshield wiper and washer commonly used on cars could minimize the need for this manual cleaning.

Two types of lidar are mentioned in the Introduction. Both types obviously merit further testing. This testing should include realistic shipboard testing. For example, measurements could be taken from a small ship in the wintertime North Atlantic. Such measurements would be useful for modeling visibility in the maritime boundary layer and evaluating both types of lidars.

ACKNOWLEDGMENTS

I thank M.A. Vietti for initial work on the lidar, L.H. Ruhnke for his advice, and H.E. Gerber for his comments. J.C. Bailey suggested many improvements to the first draft.

REFERENCES

1. C. Warner, "Slant Range Visibility Determination from Lidar Signatures by the Two Point Method," *Opt. Laser Technol.* **13**, 27-36 (1981).

2. J.D. Klett, "On the Analytical Inversion of Lidar Returns from an Inhomogeneous Atmosphere," ASL-CR-80-0008-3, Atmospheric Sciences Laboratory, White Sands Missile Range, New Mexico, 1980 [AD-A085 922].

3. W.J. Lentz, "The Visioceilometer: A Portable Visibility and Cloud Ceiling Height Lidar," ASL-TR-0105, Atmospheric Sciences Laboratory, White Sands Missile Range, New Mexico, 1982 [AD-A113 650].

4. Sperry Rand, "Runway Visual Range/Cloud Base Height Measurement Equipment," SGD-4241-1977-1, Naval Air Systems Command, Washington, D.C., 1976

5. ANSI Z136.1, "American National Standard for the Safe Use of Lasers," American National Standards Institute, New York, 1980.

6. R. Helvey, Pacific Missile Test Center, personal communication.

7. R.T. Collis, "Lidar," in *Advances in Geophysics*, H.E. Landsberg and J. van Mieghem, eds. (Academic Press, New York, 1969), Vol. 13, pp. 113-139.

8. P.R. Bevington, *Data Reduction and Error Analysis for the Physical Sciences* (McGraw-Hill, New York, 1969).

9. "Instruction Manual for the VR-301 Visibility Meter," HSS, Bedford, Massachusetts, Feb. 7, 1983.

END

FILMED